Received: 5 March 2020 | Revised: 18 April 2020 | Accepted: 20 April 2020

DOI: 10.1002/er.5520

RESEARCH ARTICLE

INTERNATIONAL JOURNAL OF ENERGY RESEARCH WILEY

Optimization of the zinc oxide reduction in the charging process of zinc-air flow batteries

Tien-Fu Yang[1,2] | **Jhang-Cheng Chen**[1,2] | **Wei-Mon Yan**[1,2] | **Mohammad Ghalambaz**[3,4]

[1]Department of Energy and Refrigerating Air-Conditioning Engineering, National Taipei University of Technology, Taipei, Taiwan

[2]Research Center of Energy Conservation for New Generation of Residential Commercial, and Industrial Sectors, National Taipei University of Technology, Taipei, Taiwan

[3]Metamaterials for Mechanical, Biomechanical and Multiphysical Applications Research Group, Ton Duc Thang University, Ho Chi Minh City, Vietnam

[4]Faculty of Applied Sciences, Ton Duc Thang University, Ho Chi Minh City, Vietnam

Correspondence
Wei-Mon Yan, Department of Energy and Refrigerating Air-Conditioning Engineering, National Taipei University of Technology, Taipei 10608, Taiwan.
Email: wmyan@ntut.edu.tw (W.-M. Y.)

Mohammad Ghalambaz, Ton Duc Thang University, Ho Chi Minh City, Vietnam.
Email: mohammad.ghalambaz@tdtu.edu (M. G.)

Funding information
Ministry of Education; Ministry of Science and Technology, Taiwan, Grant/Award Number: MOST 106-2221-E-027-103

Summary

In practice, the zinc-air flow batteries are charging by reduction of zinc oxide, dissolved in the battery electrolyte through consuming electrical energy. Later, during the discharge process, the produced zinc reacts with oxygen and releases electrical energy. Thus, the amount of produced zinc in a battery is directly related to the amount of energy storage. The current work aims to maximize the reduction of zinc oxide for a single cell of 100 W zinc-air flow battery by using the Taguchi method. The controlling parameters, which influence the zinc production are charging current, electrolyte concentration (KOH), stirring speed of the electrolyte, and electrolyte temperature. Interestingly, the results show that the temperature of the electrolyte is the most effective parameter of zinc oxide reduction. After that, the charging current density, electrolyte concentration, and stirring speed are the other important parameters, respectively. The results reveal that an optimized set of the controlling parameters could improve the zinc production up to six-fold compared to a badly tuned set of control parameters.

KEYWORDS

alkaline electrolyte, electrolyte temperature, energy storage, zinc-air battery, zinc oxide reduction

1 | INTRODUCTION

Awareness of climate change and ever-increasing demands in energy has accelerated the inevitable transition from fossil fuels to clean renewable energy.[1] Due to the transient nature of most renewable energy sources and the variable profile of energy consumptions, energy storage is an inevitable part of renewable systems. Hence, developing and improving the efficiency of energy storage systems is an urgent task. The chemical energy storage in batteries has been an excellent way of energy storage. Since a long time ago, the batteries are being

[Correction added on 15 June 2020, after first online publication: the correspondence address of Mohammad Ghalambaz has been corrected in this version.]

used in extending applications such as electric vehicles, grid-scale energy storage, and portable electronic devices.

There are various commercial types of batteries for chemical energy storage, yet the lithium-ion batteries (LIBs) technology has dominated the consumer market due to its high power density and high specific energy.[2] LIBs have been studied in many of the literature works,[3,4] and currently, they are reaching their capacity limit as their power density is limited by the capacity of the electrode materials.[1,5] There are also excellent recent studies on further improvement of the LIBs using nanospheres,[6] nano-fibers.[7]

One of the significant disadvantages of LIBs, which is getting serious, is their safety and hazardous problem. LIBs pose high concentrations of leachable metals, which demand special treatment disposal. Moreover, their tendency to explode and catch fire is another serious problem in their usage and disposal.[8] For instance, Australia's controversial new battery installation rules, called, AS/NZS 5139:2019, regarding the safety of batteries. These rules are particularly around concerns about potential fire hazards presented by some battery chemistries, and they will significantly increase the expense of renewable energy systems.[9] The aging of LIBs is a challenging and complicated issue.[10] Thus, many researchers are aggressively seeking alternative batteries to overcome the disadvantages of LIBs and meet market demands.

Recently, metal-air batteries (MABs) have gained a revived interest due to their high energy densities. These batteries utilize the oxygen as the reactant at the positive electrode, which can be available in the air outside of the battery. Indeed, the MABs electrochemically couples an air-breathing positive electrode to a metal negative electrode through a suitable electrolyte.[2] These batteries have the features of traditional batteries by using metal as the negative electrode. The same as conventional fuel cells the MABs utilize a porous positive electrode structure. The positive electrode necessitates an inexhaustible oxygen source as the reactant. Hence, MABs can theoretically have very high energy densities up to 10-folds of LIBs.[2,11] MABs are promising alternatives to LIBs due to the advantages of safety, low cost, extremely high energy density, and abundant raw materials.[12]

Currently, much of the literature works have focused on the thermal management of battery packs. For instance, the thermal management of LIBs large battery packs,[13] uniform cooling of battery packs,[14,15] direct evaporative cooling,[16] cooling flow paths,[17] and reaction-temperature estimation inside batteries.[18] These approaches could help the improvement of the available batteries technologies. At present, new generations of batteries with high energy storage densities are demanded.

Various metals such as aluminum,[19] iron,[20] lithium,[21] magnesium,[22] potassium,[23] zinc,[24] and other metals or alloys[25] are utilized for metal-air/oxygen batteries. The electrolyte is also an important aspect of MABs, which has been addressed in some of the recent studies, such as using hybrid electrolytes[26] and gel-based electrolytes.[27] Many recent patents have also been filed very recently. For instance, MABs with an air supply[28] or purification[29,30] module, zinc-air batteries,[31] flow batteries,[32] and fully electrically rechargeable metal-air battery systems[33] are a few examples of patents since 2018. Kear et al[34] carried out a review study on the energy storage of flow batteries considering the technological, financial, and policy aspects while Yuan et al[35] reviewed the durability of redox flow batteries.

Among various possible candidates for the metal-air batteries, the zinc-air batteries are of special interest. The theoretical specific energy density of a zinc-air battery can reach 1218 Wh/kg thanks to the supply of reactive oxygen in the surrounding air.[12] Although aluminum-air or lithium-air batteries can produce a theoretical higher energy density rather than that of zinc-air batteries,[36] the zinc is a metal with a higher reaction activity with oxygen. Moreover, zinc can be electrodeposited in conventional aqueous electrolytes such as alkaline, and hence, it can be handled safely in a humid atmosphere and oxygen. Zinc is also abundant in nature, and its cost is fair.[37-39]

Hence, zinc is a promising candidate for future MABs. Some promising researches on various aspects of zinc flow batteries have been performed. Mainar et al[40] provided a comprehensive review of progress in electrolytes for zinc flow batteries. Wang and Yu[41] presented a model for the aging of rechargeable zinc-air batteries while Chladil et al[42] addressed the impact of the presence of organic additives on the zinc oxide reduction in zinc-based secondary cells. They focused on the morphology of deposited zinc and found that the presence of additives influences the crystallography of the deposited particles from basal texture to pyramidal.

Although MABs are promising candidates with high potential of power density energy storage, the practical application of these batteries requires researches at various aspects. The discharging rate of these batteries is limited to the supply of oxygen at the cathode. Their charging efficiency and mechanisms of metal oxide reduction shall be significantly improved. In Zn-air flow batteries, the reaction of the ZnO with oxygen produces electrical energy. The metal oxide (ZnO) later shall be reduced to pure metal (Zn) in a charging process. Hence, the reduction of ZnO is an essential stage in the charging

of Zn-air batteries. An efficient reduction of ZnO during the charging process can significantly affect the efficiency of a Zn-air battery.

The literature review shows that electrolyte concentration,[43] electrolyte operating temperature,[44] electrodeposition time,[45] electrodeposition current density[45] are some affecting parameters on the production and grain shape control of metals. The circulation flow rate of the electrolyte can be adjusted in a zinc-air battery with a forced convection flow of electrolyte. Hence, the string speed or electrolyte motion can be another effective parameter. In our previous study, we investigated the effect of using a pulse current on the ZnO reduction productivity for Zn-air battery applications[46] in a very highly concentrated and high speed circulated zinc oxide electrolyte. The results show that using a fine-tuned pulse current is an efficient way for the charging of zinc-air batteries, which can notably improve the charging efficiency of a zinc-air battery.

Following Reference 46, the current research aims to address the impact of control parameters to maximize the ZnO reduction in a KOH electrolyte, experimentally. The control parameters are the electrolyte concentration, stirring speed, charging current, and electrolyte temperature. The Taguchi optimization method was employed to adjust the control parameters optimally and maximize the efficiency of ZnO reduction for Zn-air batteries.

2 | EXPERIMENTAL SETUP AND METHOD

The actual image of a Zn-air flow battery pack consists of six zinc oxide reduction modules, which are assembled in a lab-scale for a 100 W energy storage system. As all of the modules functions are the same, in the present study, one of the modules is selected as the case study to avoid unnecessary complications and focus on the zinc oxide reduction performance. The present experiment aims to study and optimize the zinc oxide reduction for four control variables of electrolyte concentration, electrolyte operating temperature, electrolyte stirring speed, and current density.

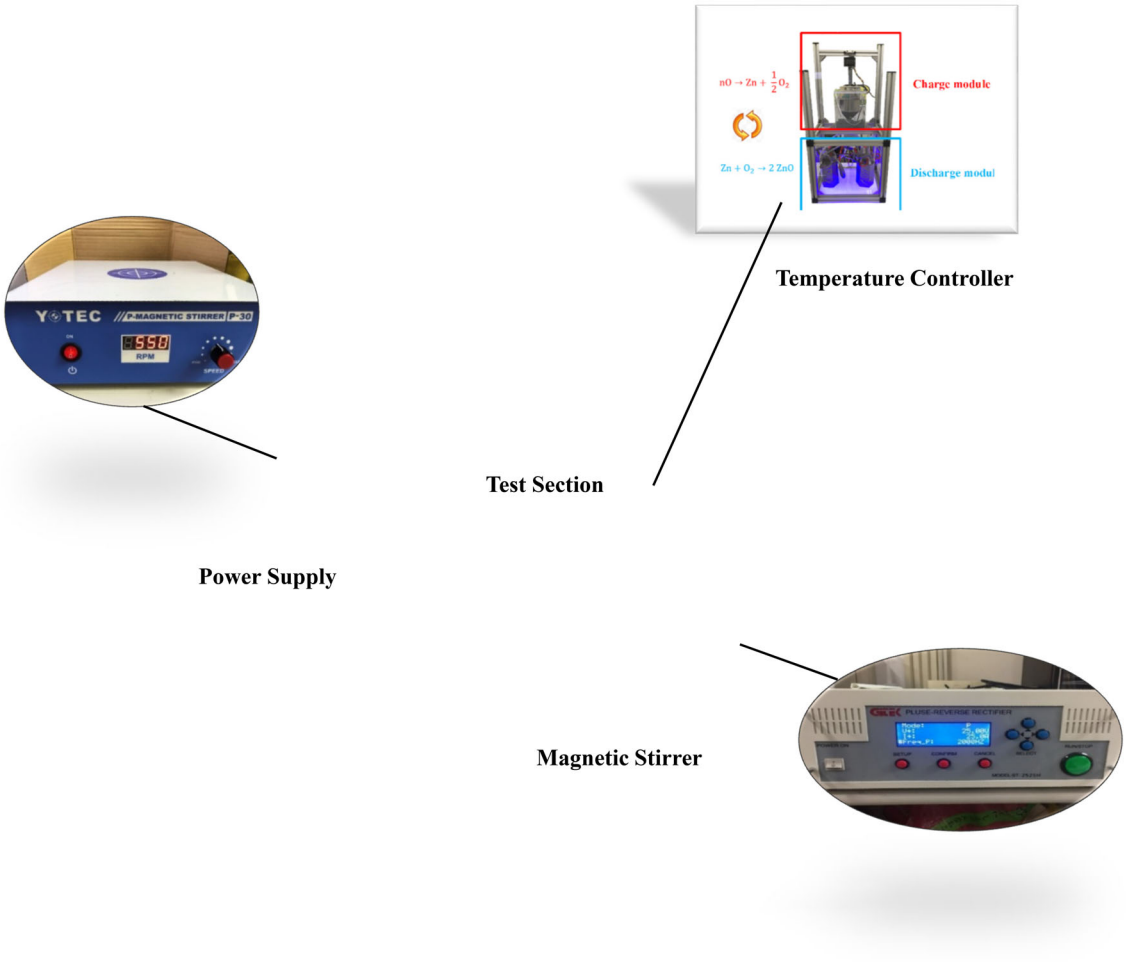

FIGURE 1 Schematic diagram of the experimental setup [Colour figure can be viewed at wileyonlinelibrary.com]

2.1 | Experimental procedure and materials

Figure 1 illustrated a schematic diagram of the experimental setup of this study. The setup consists of an electrolyte tank, an automatic temperature controller, an intelligent power supply, and an adjustable magnetic stirrer. An image of the practical complete Zn-air flow battery with six cells is shown in Figure 2A.

The anode and cathode were made by high conductivity C1100 toughened copper TCU (purity of 99.90% made by Gitek Electronics Co.) for the electrochemical deposition. The diameters of the anode and cathode poles are 19 mm, and their lengths are 100 mm. A view of the anodes and cathode electrodes is depicted in Figure 2B. The top section of the anodes and cathodes was drilled with M6-size holes to a depth of 20 mm at the center to ensure a good electrical connection between roads. Thus, the circuit wires could be connected to the poles properly.

The alkaline electrolyte can damage pure copper; hence, to ensure that the copper rods are smooth and uniform during the experiments, the surface of the toughened copper was treated by a professional electroplating manufacturer (Xuemei precious metal electroplating factory). A view of the treated copper rod with a layer of rhodium is depicted in Figure 2C. A measuring cup made of glass with a capacity of 3000 mL was employed as the electrolyte container. The top cover of the container, including positions for mounting of the anode and cathodes, was printed using a 3D printer (Ultimaker 3 Extended; 3DMart Co.). The 3D-printed cover ensures a fixed relative distance between the cathode and anode during the tests. The space between the center points of the two holes was 40 mm, and both of the cathode and anode were fixed to the rear of the top cover. The shortest and longest separation between the cathode and anode were 21 mm and 59 mm, respectively. A view of the top cover and mounted anode and cathode is illustrated in Figure 2D.

The electrolyte for electrochemical deposition was synthesized using potassium hydroxide (KOH, First Chemical Co.). Different weights of 368.42, 421.05, 473.68, and 526.31 g of 95% potassium hydroxide particles were respectively utilized to produce different electrolyte concentrations including 35 wt% (8.5 M), 40 wt% (10.1 M), 45 wt% (11.7 M), 50 wt% (13.5 M) for the experiment. The zinc oxide particles (First Chemical Co.) with a purity of 99.7% were used in the electrolyte.

In the preparation of the electrolyte of potassium hydroxide, the particles of KOH are dissolved in water. The container of KOH and water was stirred at a speed of 500 rpm on top of a magnet mixer (P-30, Yeong-Shin Co.). Due to the pungent odor and exothermic phenomenon through the synthesize of the solution, it was placed in the fume hood. An automatic electrical heater (SM5-LCD) was employed to measure and adjust the temperature of the solution before and during the experiment.

This experiment has a variety of control variables such as electrolyte concentration, electrolyte operating temperature, electrolyte stirring speed, and current density. During each experiment, the voltage was recorded and monitored carefully. A voltage threshold of 2.5 V is an essential parameter in the present study. At a voltage higher than 2.5 V, the hydrogen production evolves in the experiment, and it notably reduces the performance of zinc production. The production of hydrogen will change the concentration of the electrolyte and makes

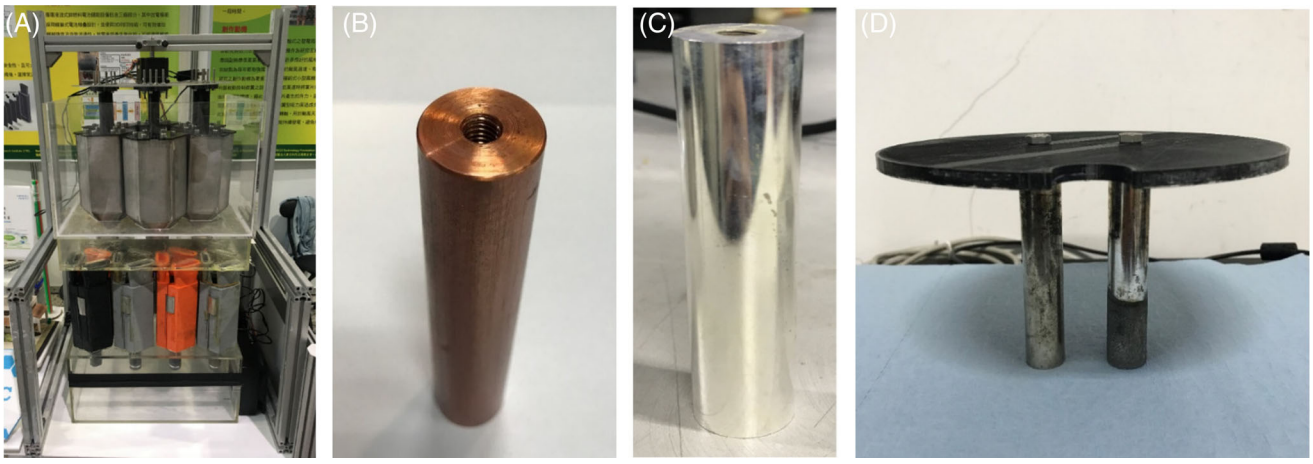

FIGURE 2 The actual Zn-air battery and the anode and cathode of the experiment: (A) six charging cells of Zn-air battery, (B) C1100 TCU, (C) C1100 TCU with rhodium plated on the surface, (D) during the experiment [Colour figure can be viewed at wileyonlinelibrary.com]

the experiment invalid. Hence, the maximum voltage shall be below 2.5 V during all of the experiments and for any current and temperature. Due to the safety risks of the experiment, earing test clothes, masks, alkali-resistant plastic gloves, and using controlled environment ventilated cabin are mandatory.

The detailed experimental steps can be summarized in Figure 3A. The chart of the test steps is shown in Figure 3B. As the first step, zinc oxide is mixed into the electrolyte using a magnet mixer, and the electrolyte is heated and uniformly mixed for at least 3 hours. The top cover, including the cathode and anode, placed on the container. The poles are immersed in the electrolyte and connected to the intelligent power supply (ST-2525H, Gitek Electronics Co.). The circuit connectivity tested by an ohmic impedance meter to ensure good electrical connection between the various parts of the electric circuit.

Then, the electrochemical deposition experiment commenced by feeding an adjusted constant current to the circuit and recording the experiment time. The electrodepositing time was fixed as 60 minutes for all experiments. During the experiment, the voltage was carefully monitored to ensure safe voltage lower than 2.5 V. After 60 minutes of electrodeposition, the top cover was removed, and the deposited zinc (produced zinc during the zinc oxide reduction procedure) scraped from the cathode and collected in a beaker. The beaker was transferred into a vacuum dryer (DOV-30 N; Yeong-Shin Co.) and maintained for at least 3 hours at 80°C. The drying process removes all of the moisture from the sample.

The post-processing diagram of the experiment is illustrated in Figure 4. As seen, the dried zinc was transferred to a plastic vacuum container (PC-210; Yeong-Shin Co.) to stop possible zinc reaction with atmospheric oxygen. The vacuum was maintained by a vacuum pump (90 W; Yeong-Shin Co.) at the oven and plastic vacuum dish.

Finally, an electronic balance (EHB + 150; accuracy: 0.001 g; T-Scale Co.) is utilized to measure the weight of the extracted Zn. The experiment steps were repeated for each set of experiment parameters.

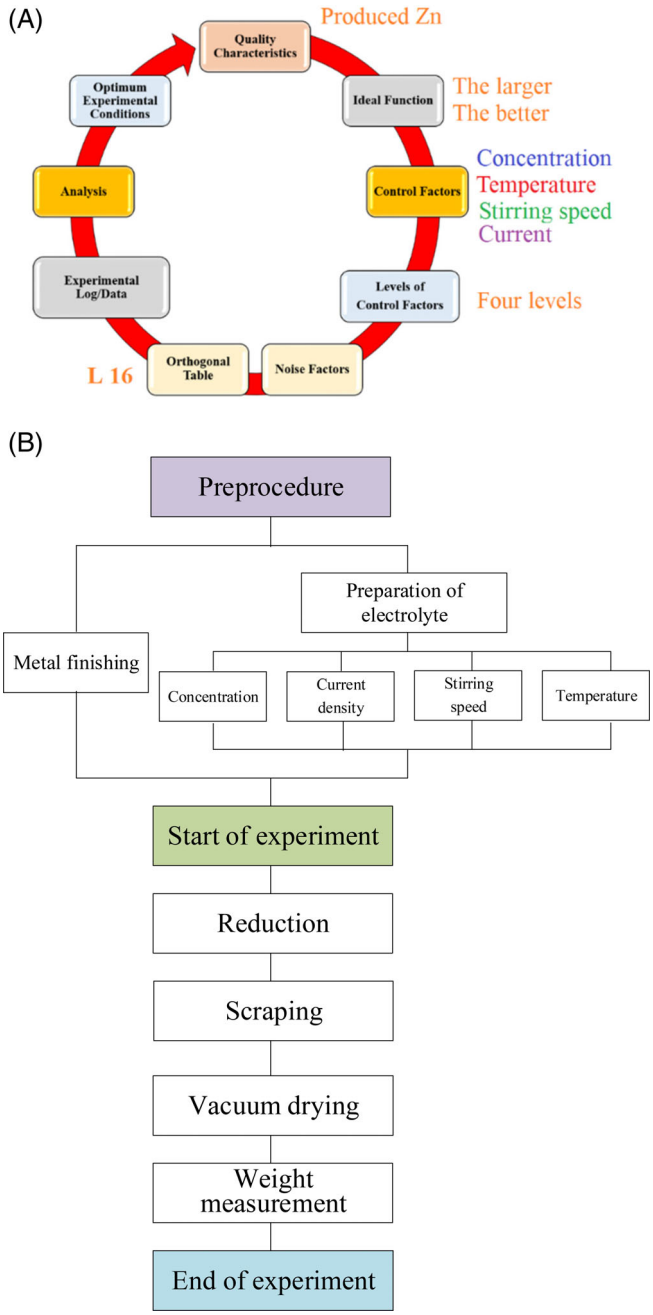

FIGURE 3 The steps of the Taguchi method and implementation of the experiments: (A) Taguchi method and its implementation steps, (B) the test steps of the experiment [Colour figure can be viewed at wileyonlinelibrary.com]

3 | THE TAGUCHI OPTIMIZATION METHOD

The Taguchi method was developed by Taguchi.[47] Taguchi proposed a three-step approach for the optimization of a product or a process. These steps are system design, parameter design, and tolerance design. The system design presents an early stage of a system or a product, which has been produced based on scientific and engineering knowledge. The system design stage is an early stage of a product or process and is far from an optimized cost or quality. Hence, the next step is parameter design. In this step, the parameters of a system shall be adjusted to improve the product or process.[48]

Optimization of the control parameters leads to an improved system quality or cost. Finally, tolerance design is employed to identify tolerances around the optimal settings achieved in the parameter design step. The tolerance design step is only essential when the parameters, achieved by parameter design, could not provide the

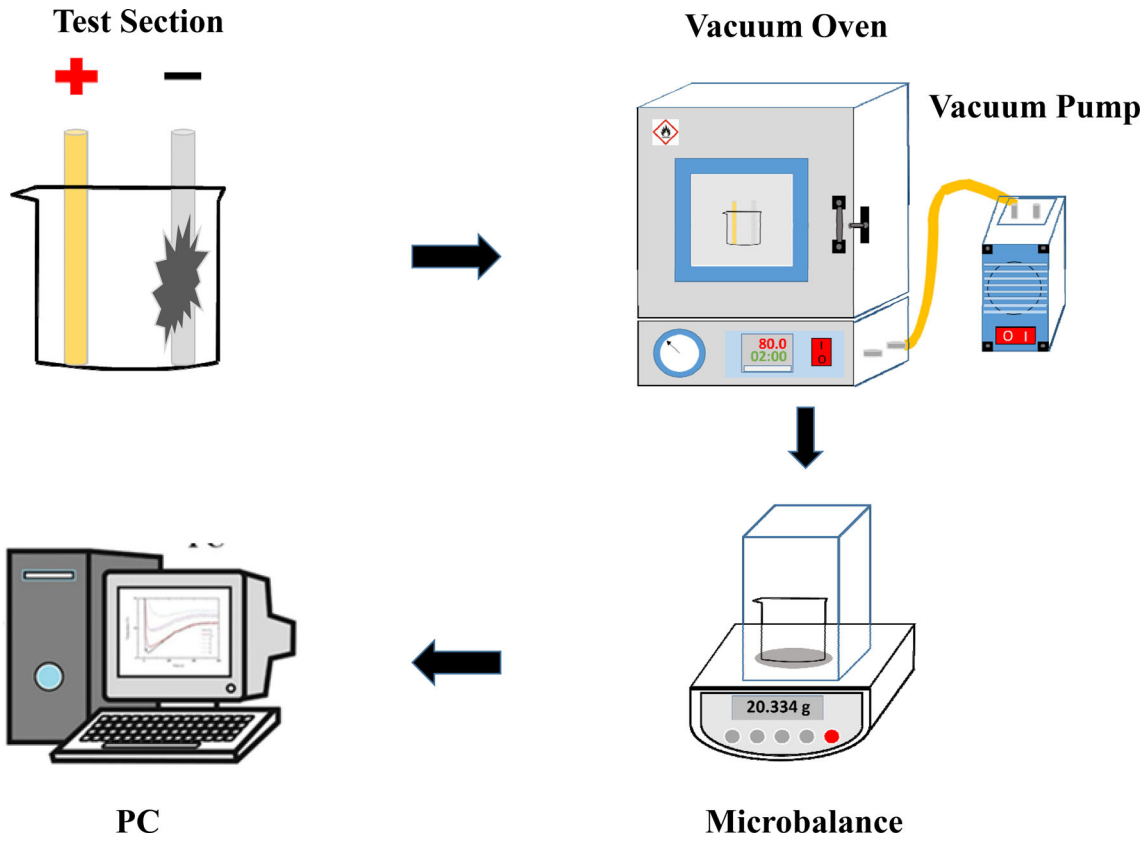

FIGURE 4 Post-processing diagram of the experimental system [Colour figure can be viewed at wileyonlinelibrary.com]

expected performance.[49] Considering the above steps, the parameter-design step is the key step in the Taguchi method for a low-cost and high-quality product or process.

Performing and optimizing for control parameters by exploring all of the possible combinations of the variables requires many tests. In practice, the experimental tests are time-consuming and expensive. Hence, Taguchi introduced a method to explore the combination of control parameters in a reduced orthogonal space. This approach significantly reduces the number of required experimental tests.[48] Taguchi recommends the utilization of a signal to noise (S/N) ratio to size the quality characteristics differing from the preferred values. A quality characteristic can be represented in various desired forms. For example, the quality characteristic of the current work can be introduced as the higher zinc oxide reduction the better. Considering the higher the better approach, the S/N ratio can be evaluated as:

$$\mathrm{S/N} = -10\log_{10}\left(\frac{1}{n}\sum_{i=1}^{n}\frac{1}{Yi^2}\right), \quad (1)$$

where Y and n indicate the respective characteristic and the number of test data, respectively. A higher S/N denotes a better quality; hence, an optimal value of a process parameter can be expected at the highest S/N ratio. Therefore, the optimum combination of control parameters corresponds to the highest S/N value can be considered as the optimum parameters of a process. A confirmation experiment using the optimal process parameters is recommended to ensure the optimal process.

The steps of Taguchi optimization method for parameter design stage can be summarized as (a) selection of important design parameters and the quality characteristics; (b) selection of discretization of the range of the control parameters into a finite number of parameter levels and determination of the possible interactions between the control parameters; (c) identification of an adequate orthogonal array of the control parameters; (d) performing experiments for the array of the control parameters; (e) examination of the experimental results by employing the S/N approach; (f) identification of maximum S/N for the control parameters; and (g)

experimenting with the optimal set of control parameters for verification.[48,49]

When using the Taguchi orthogonal table planning, it is necessary to have clear quality characteristics and control parameters. In this study, the weight of produced zinc is adopted as a quality characteristic. The higher produced zinc, the better the quality. The control parameters are electrolyte concentration, electrolyte operating temperature, electrolyte stirring speed and current density, and each of them is discrete into four levels. An orthogonal array of the discretized control parameters of L16 table was produced. This table shows the design parameter factors and varying levels of zinc oxide reduction for energy storage. The commonly applicable table for reducing the number of experiments is using orthogonal Taguchi tables.

The orthogonality lets the factors to be computed individually and independently, and when the factors themselves change, it does not affect the evaluation of other factors and all other combinations. Each level combination has the same number of occurrences, in which four control parameters are involved in the present study. Each control parameter is divided into four levels. Hence, a standard L16 Taguchi table is adopted. The electrolyte concentration ranges from 35 to 50 wt% (8.5 to 13.5 M), while the electrolyte temperature considered in the practical range of 30°C and 60°C. The electrolyte stirring speed is adjusted between 700 and 1000 rpm, and the charging current is in the range of 0.9 to 1.5 A. Table 1 shows the control parameters L16-table of Taguchi. For each set of the controlling parameters, introduced in Table 1, the experiments were performed three times.

4 | RESULTS AND DISCUSSION

The weight of zinc production was experimentally measured and reported in Table 2 for each set of control parameters of Table 1. As the experiment was repeated for three times, there are three columns for the measured zinc weights. Table 2 demonstrates the effects of electrolyte concentration, electrolyte temperature, electrolyte stirring speed, and current density on zinc oxide reduction.

4.1 | Taguchi S/N study

The S/N values are computed using Equation (1) and reported in Table 2. Now, the results of Table 2 can be

TABLE 1 The corresponding level control parameters of Table 1

	Factor			
	A	B	C	D
Case	Electrolyte concentration (wt%)	Temperature (°C)	Stirring speed (rpm)	Current (A)
1	35	30	700	0.9
2	35	40	800	1.1
3	35	50	900	1.3
4	35	60	1000	1.5
5	40	30	800	1.3
6	40	40	700	1.5
7	40	50	1000	0.9
8	40	60	900	1.1
9	45	30	900	1.5
10	45	40	1000	1.3
11	45	50	700	1.1
12	45	60	800	0.9
13	50	30	1000	1.1
14	50	40	900	0.9
15	50	50	800	1.5
16	50	60	700	1.3

Note: Current density = current/reaction area (reaction area: 0.4176 dm^2).

TABLE 2 The produced zinc in the battery and the S/N ratio for each set of experiments

	Factor					
	Experiment Set 1		Experiment Set 2		Experiment Set 3	
Case	Zinc particle weight (g)	S/N (η) (dB)	Zinc particle weight (g)	S/N (η) (dB)	Zinc particle weight (g)	S/N (η) (dB)
1	1.769	4.9546	1.657	4.38645	1.462	3.29895
2	1.545	3.7786	1.392	2.87278	1.235	1.83334
3	1.233	1.8193	1.196	1.55462	1.191	1.51824
4	0.504	−5.9514	0.412	−7.70206	0.401	−7.93711
5	1.04	2.2387	1.251	1.94515	1.212	1.67005
6	2.64	8.4321	2.362	7.46560	2.256	7.06678
7	0.783	−2.1248	0.695	−3.16030	0.634	−3.95821
8	1.371	2.7407	1.302	2.29222	1.188	1.49633
9	3.21	10.1301	2.987	9.50470	2.899	9.24496
10	2.073	6.3320	1.886	5.51083	1.821	5.20620
11	0.922	−0.7054	0.870	−1.20961	0.665	−3.54357
12	0.53	−5.5145	0.417	−7.59728	0.406	−7.82948
13	1.293	2.2320	1.289	2.20506	1.016	0.13787
14	0.533	−5.4655	0.492	−6.16070	0.474	−6.48443
15	1.109	0.8986	1.083	0.69257	0.947	−0.47300
16	0.552	−5.1612	0.536	−5.41670	0.483	−6.32106

used to draw the S/N ratio graphs and estimate the optimal set of control parameters using the Taguchi method. The corresponding S/N ratios are also plotted in Figure 5.

Figure 5A illustrates the effect of electrolyte concentration on zinc oxide reduction using the four-level S/N for the average of three experimental tests. Figure 5A shows that the electrolyte concentration 40 wt% (10.1 M) and 45 wt% (11.7 M) can provide good energy storage. Moreover, the concentration of 40 wt% (10.1 M) is better than 45 wt% (11.7 M). When the electrolyte concentration is as high as 50 wt% (13.5 M), the reduction benefit is significantly reduced. The reason is that the electrolyte concentration affects the amount of OH^- in the solution. Not always a higher concentration can be used to obtain better zinc oxide reduction. Therefore, the optimum electrolyte concentration must depend on a series of factors, which can be identified by experiments. Therefore, as the experimental results demonstrated, the zinc oxide reduction performance is best when the electrolyte concentration is maintained between 40 wt% (10.1 M) and 45 wt % (11.7 M).

Figure 5B denotes the influence of electrolyte temperature on zinc production, that is, energy storage. The temperature selection of the electrolyte starts at 30°C and takes a value of 10°C every interval. Thus, the experimented levels of the temperature for potassium hydroxide electrolyte are 30°C, 40°C, 50°C, and 60°C. After calculating the average value of the three experimental electrolyte temperatures, the four-level S/N of a response graph is plotted in Figure 5B. It can be observed that the electrolyte temperature of 30°C is the optimum value, and as the temperature increases, the zinc production starts to decline.

It is worth noting that an electrolyte temperature of 60°C, regardless of the magnitude of other variables, produces stiff and blocky zinc particles on the cathode surface, which was hard to scrap. The reason was that a rise in the temperature of the solution would speed up the rate of cathodic electrodeposition reaction and the diffusion rate of ions. Also, it can increase the conductivity as well as the upper limit of current density and reduce the polarization at the cathode end, but it will also make the crystal of the coating layer thicker and harder.

The trend of the outcomes in Figure 5B reveals that the electrolyte temperature is an important parameter, which significantly controls the reduction of zinc oxide. Selecting the correct working temperature for electrolyte increases the amount of the produced zinc particles and softens the zinc particles over the cathode surface; otherwise, the opposite effect will be obtained. The mechanical scraping of produced particles is a crucial design aspect as, in many practical applications, mechanical scraping

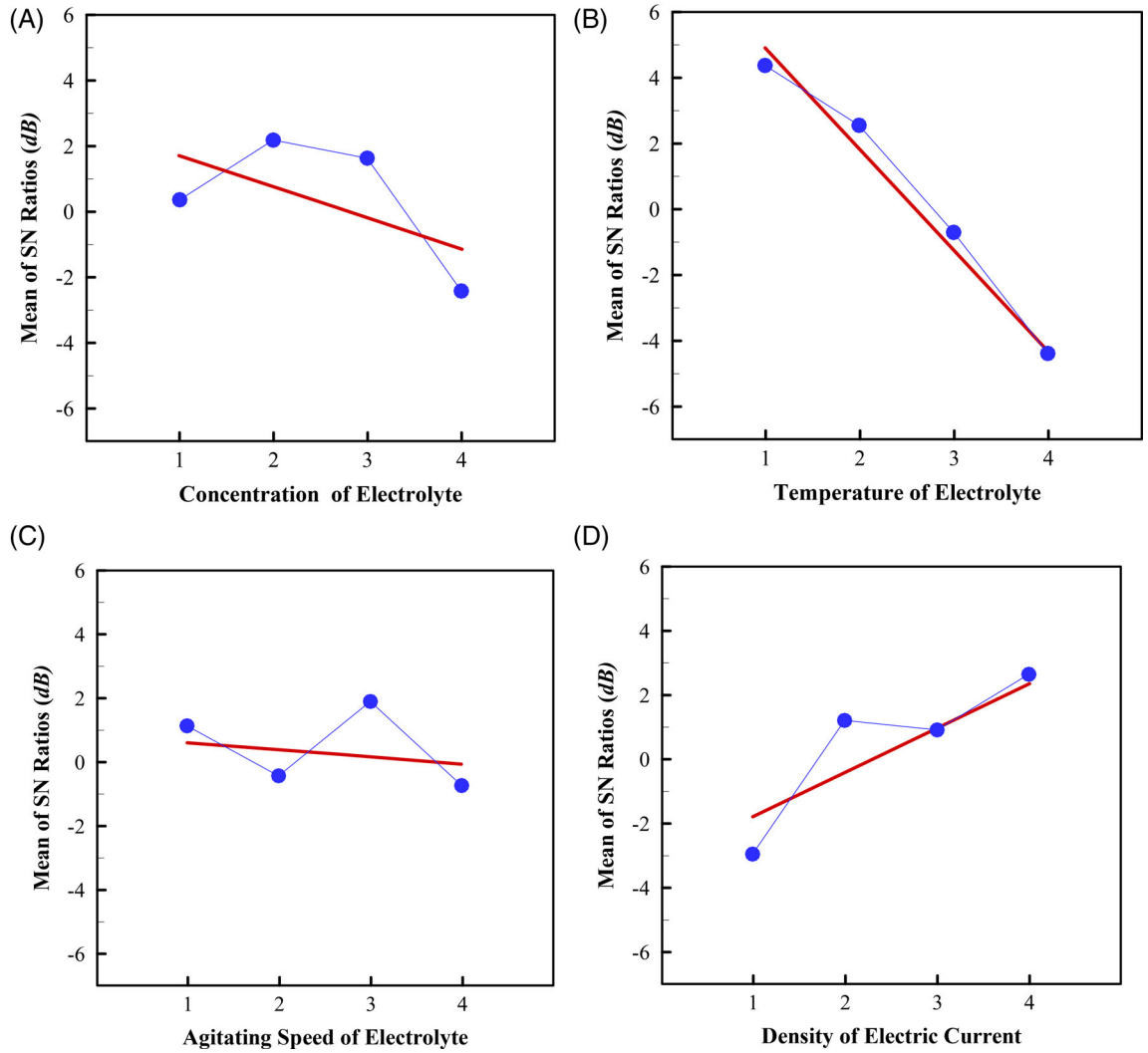

FIGURE 5 Response diagram of the control parameters: (A) electrolyte concentration, (B) electrolyte temperature, (C) electrolyte stirring speed, (D) current density [Colour figure can be viewed at wileyonlinelibrary.com]

of the zinc particles can be a part of the energy storage system. Hence, the controlled temperature of 30°C would not only provide a higher amount of zinc but also produce a soft texture and easy to scrap zinc particles. A soft and easy to scrap zinc particles are desired for flow battery systems.

Figure 5C shows the effect of electrolyte stirring speed on the produced zinc particles. The four levels of the stirring speed of the electrolyte are selected as 700, 800, 900, 1000 rpm. Figure 5C displays the S/N values against various magnitudes of stirring speeds. As seen, the electrolyte stirring speed of 900 rpm is the optimum value. With the increase of the stirring speed, there is no significant difference in the benefits of zinc oxide reduction, and the average S/N of the four levels is above 0 dB. Stirring the electrolyte can reduce the polarization reaction at the cathode end. Therefore, as long as the electrolyte is uniformly stirred, the zinc oxide in the electrolyte, which was reduced to zinc at the vicinity of the cathode surface, would be replaced immediately. Therefore, the stirring speed is only relevant when there is a gradient of zinc oxide concentration next to the cathode surface. Hence, some degrees of stirring could remove the concentration gradients, and as a result, the effect of the stirring speed is minimal in a well-stirred electrolyte.

Figure 5D shows the influence of the current density on the produced zinc for energy storage. The current starts at 0.9 A and takes a value of 0.2 A every interval. A total of four levels are considered as 0.9, 1.1, 1.3, and 1.5 A. As the reaction area is 0.4176 dm^{-2}; these currents can be converted to current densities as 2.155, 2.634, 3.113, and 3.592 A/dm^2, respectively.

A four-level S/N average of three experimental current densities is calculated and plotted in Figure 5D. This figure exhibits that the extracted zinc increases first and then decreases slightly with the increase of current in the

range of 1.1 to 1.5. The reason for the rise and the slight decrease may be caused by the fact that the Taguchi method is affected by the interaction of other parameters. Generally, an increase in current improves zinc production. However, it should be noted that the current density of each electrolyte has a limit of the upper limit and the lower limit. The quality of the coating will begin to deteriorate, if the excessive current density exceeds the upper limit. In such a case, the phenomenon of burnt blackening will occur.

4.2 | Taguchi analysis and optimization solution

By combining the optimal values of the electrolyte concentration, electrolyte temperature, electrolyte stirring speed, and current density, which were discussed in the above section, an optimal level for each reference variable can be achieved. Based on the results of Figure 5, the optimal liquid concentration is at the second level (40 wt%), the electrolyte temperature is at the first level (30°C), the electrolyte stirring speed is at the third level (900 rpm), and the current density is at the fourth level (3.592 A/dm^2).

The estimated optimized set of the Taguchi method was tested experimentally, and 3.343 g zinc was produced. As depicted in the L16 Table 1, the best combination of the Taguchi method is the parameters of the ninth group: the electrolyte concentration of 45 wt% (11.7 M), the electrolyte temperature of 30°C, the electrolyte stirring speed of 900 rpm, and the current density of 3.592 A/dm^2. The weight of the extracted Zn is 3.21 g.

It is interesting that only one reference variable-electrolyte concentration: 40 wt% (10.1 M) and 45 wt% (11.7 M) was changed among the two experimental parameters, and the weight of the obtained zinc was increased by only 0.133 g. Figure 5A also shows that the changes in the electrolyte concentration from 40 wt% (10.1 M) to 45 wt% (11.7 M) only slightly affects zinc production.

4.3 | The importance of each control parameter on the energy storage

The significance of the control parameters is ranked in Table 3 using the S/N ratio of the Taguchi method. The value of the Delta column refers to the difference between the maximum and minimum values of the S/N average of the four conditions of each parameter. For instance, the Delta in column A is (2.1754) − (−2.4430) = 4.6184. The other values of the table are computed similarly. The rank value was utilized to sort the Delta by magnitude. As depicted in Table 3, the rank of the electrolyte temperature is 1, indicating the highest impact of the temperature on zinc production. Here, the control parameters are ranked from the most influential parameter to less important one as electrolyte temperature, current density, electrolyte concentration, and the stirring speed of the electrolyte, respectively.

4.4 | Electrodeposition surface type and surface element analysis

The scanning electron microscope used in this experiment was Carl Zeiss AG model JEOL JSM-6500F. Scanning electron microscopy is performed by point-by-point scanning on the surface of the sample by a focused electron beam. Three cases of the best performance (a), intermediate performance (b), and worst performance (c) for zinc production are selected as samples for surface study. In this regard, the following sets of L16 tables are adopted ninth group (a), the third group (b), and the sixteenth group (c). The shooting magnifications are 1000, 3000, and 8000 times; the results are depicted in Figures 5-7.

At 1000 times, the particles in Figure 6A belong to the agglomerated form, and they are smooth and sticky, and some separated single tips are notable. The formation of the particles in Figure 6B is prominent. It is also very straightforward to see that there are concave holes between the particles and the particles, and each particle does not stick to the adjacent particles to

TABLE 3 Response tables for the quality characteristics of zinc particles

No.	Electrolyte concentration	Electrolyte temperature	Stirring speed	Current density
Level 1	0.3689	4.3290	1.1039	−2.9713
Level 2	2.1754	2.5323	−0.4570	1.1775
Level 3	1.6274	−0.7243	1.8492	0.9080
Level 4	−2.4430	−4.4085	−0.7675	2.6143
Delta	4.6184	8.7375	2.6167	5.5856
Rank	3	1	4	2

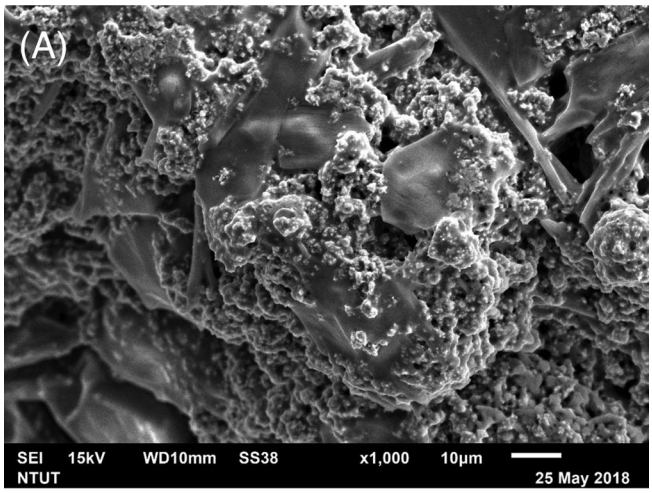

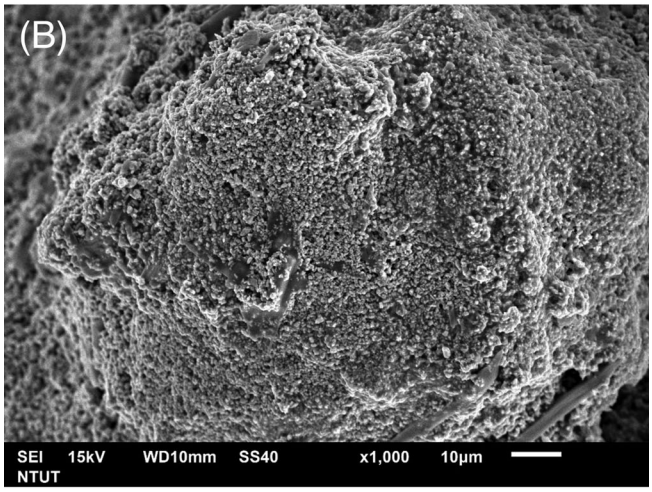

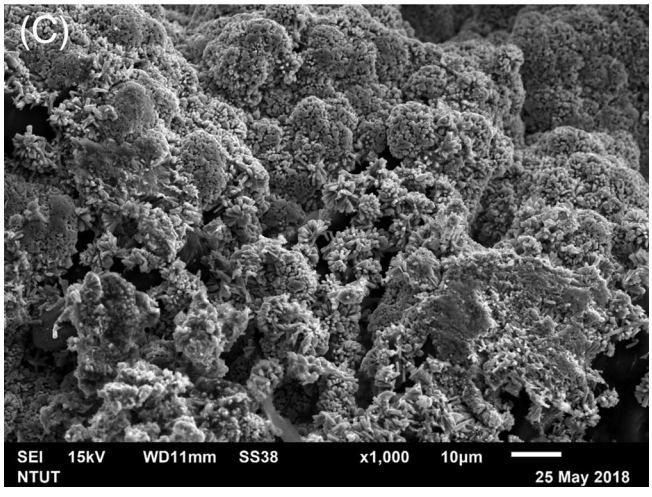

FIGURE 6 Zinc particle appearance at 1000 times of magnifications for the following group results of Table 1: (A) Group 9, (B) Group 3, (C) Group 16

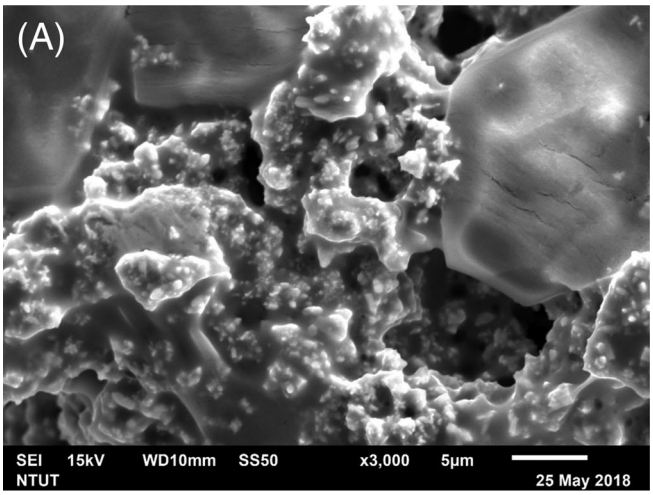

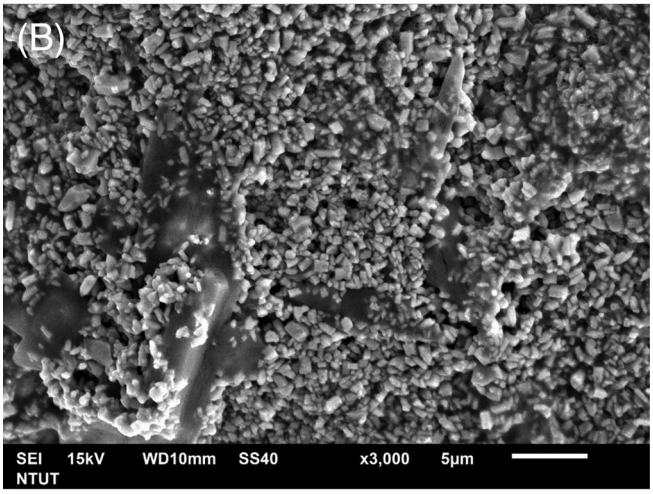

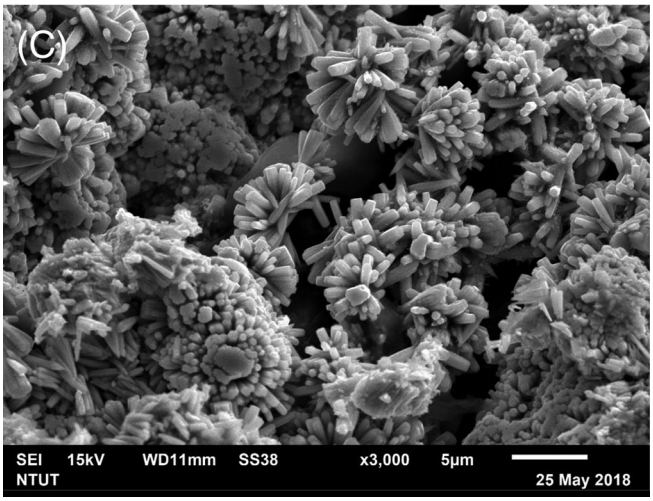

FIGURE 7 Zinc particle appearance at 3000 times of magnifications for the following group results of Table 1: (A) Group 9, (B) Group 3, (C) Group 16

produce a smooth surface like Figure 6A. In Figure 6C the particle appearance of zinc is also pronounced, but in particular, each particle is smoother than the particles of Figure 6B. Figure 6C denotes a significant gap formation between the particles instead of the depressed holes.

The surface texture for magnification of 3000 times is illustrated in Figure 7. Figure 7A shows that the particles are like clay-shape joints, and the sharp corners will squeeze out in branches. Figure 7B depicts a state, similar to the crystallization of many squares with positive tangent angles. Compared with Figure 7A, the zinc particles have a slightly different appearance. The zinc particles in Figure 7C have obvious differences. The square particles become a long version of square-square particles, and the slender particles are combined with the particles to have a crystal flower appearance, and there is also a clear gap between each flower and flower.

The magnification of 8000 times is displayed in Figure 8. The growth of the three patterns can be easily observed in these figures. In Figure 8A, the appearance is not yet clear, but some square zinc particles are ready to be formed. In Figure 8B, the particles are square shape, while some of the longer-form particles are seen in Figure 8C. In Figure 7, with the magnification of 3000 times, a similar flower shape pattern was also observed while there were some thin rectangular zinc particles in each flower. The particles are sticky to each other, and there is no appearance of the circular agglomeration. A comparison between the optimized case of Reference 46 for oscillating current and Figure 7A show that the textures of the present work are much coarser, and the numbers of produced branches are also lower in the current work.

5 | CONCLUSION

In recent years, there has been an increase in the research on liquid-flow zinc-air batteries, but most of them have discussed the discharge curve of batteries, and there are few studies related to the energy storage of Zn-air batteries. However, the commercial application and development of zinc-air batteries demand research in all aspects of these promising chemical energy storage batteries. The present research explored the parameters affecting the energy storage in zinc-air flow batteries. The various control factors were tested, and the zinc production was optimized by using the Taguchi method. The major findings of the present work can be concluded as follows:

1 The best zinc production was obtained for the electrolyte concentrations of 40 wt% (10.1 M KOH) and 45 wt % (11.7 M KOH).
2 When the temperature of the electrolyte is 30°C, the effect of reducing zinc oxide is better, and the zinc particles are soft; on the contrary, when the temperature is higher, the product is significantly reduced, and the zinc particles are stiff and blocky and difficult to scrape.

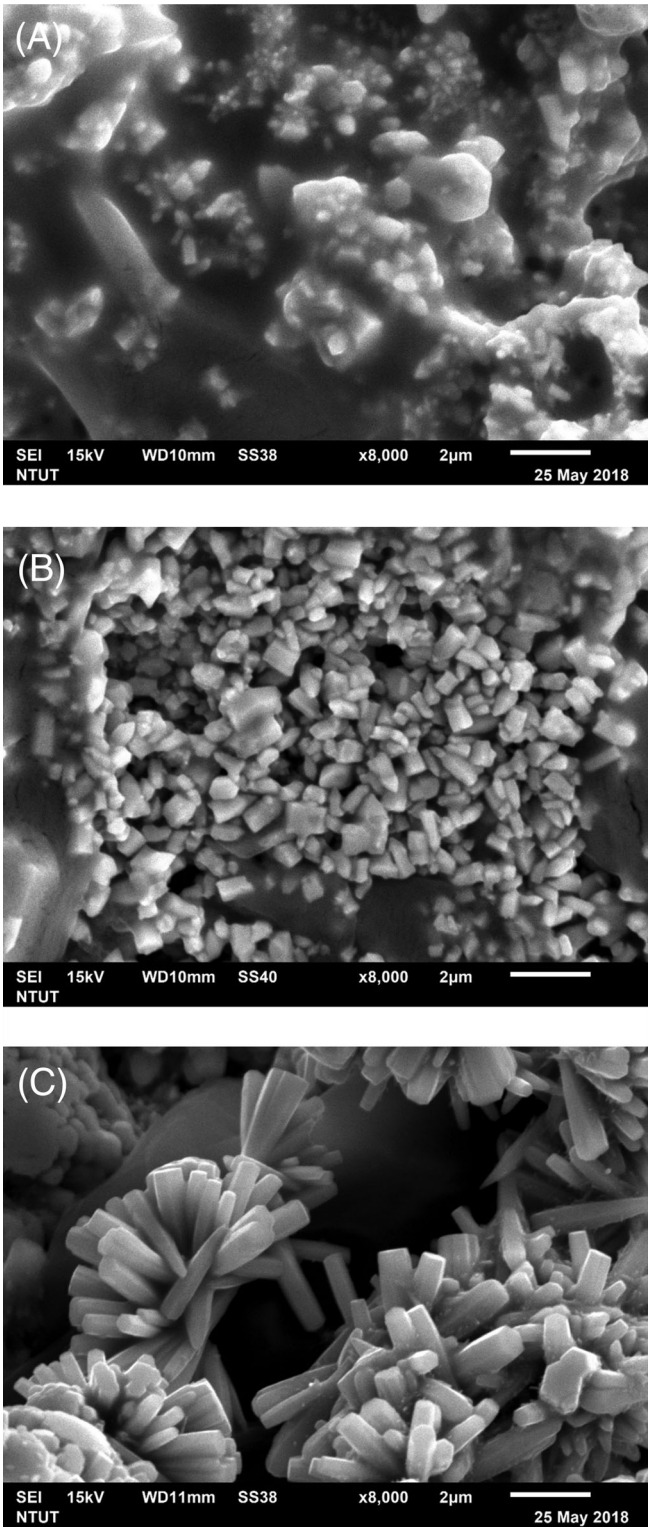

FIGURE 8 Zinc particle appearance at 8000 times of magnifications for the following group results of Table 1: (A) Group 9, (B) Group 3, (C) Group 16

3 When the electrolyte is evenly stirred, and no sediment is generated, the variation of the stirring speed induces a minimal effect on zinc production.

4 The reduction benefit of zinc oxide improves with the increase of current density, but the voltage should be controlled within the limit of 2.5 V.
5 The order of important controlling parameters, influencing the zinc production, is electrolyte temperature > current density > electrolyte concentration > electrolyte stirring speed.
6 Using the Taguchi method, the optimized set of the controlling parameters is obtained as electrolyte concentration of 45 wt% (11.7 M), electrolyte temperature of 30°C, electrolyte stirring speed of 900 rpm, current density of 3.592 A/dm^2 (1.5 A). An experiment was performed for this Taguchi optimum case, and the weight of the extracted Zn was measured 3.343 g.
7 The optimized energy storage and reduced zinc in the present study were promising. Poorly tuned controlling parameters result in zinc particle production about 0.5 g, while an optimized set of well-tuned controlling parameters could improve the weight of the collected zinc to 6-fold improvement (3.343 g).

The results of the present study revealed that the temperature of the electrolyte is the most important controlling parameter for energy storage. In the current work, a wide range of temperatures (30°C-60°C) was adopted to find the trend of the temperature effect. Thus, the temperature levels were 30, 40, 50, and 60°C. In future works, a narrower range of temperatures can be adopted to fine-tune the electrolyte temperature.

The influence of the charging current was also found significant in the weight of produced zinc. The study of Yang et al[46] demonstrated that using an optimized pulse current, instead of a uniform DC, could improve the energy storage and weight of the produced zinc particles. A combination of control parameters of the current study and the pulse current of Reference 46 is promising to provide more controlling parameters with an opportunity for better efficiency of optimized zinc oxide reduction and energy storage. Thus, performing an experimental optimization for a combination of pulse current parameters, electrolyte temperature, electrolyte concentration, and stirring speed can be subject to future studies to improve the ZnO reduction further.

ACKNOWLEDGEMENTS

The authors appreciate the financial support from the Ministry of Science and Technology, Taiwan, under grant number MOST 106-2221-E-027-103. They also appreciate the financial support by the "Research Center of Energy Conservation for New Generation of Residential, Commercial, and Industrial Sectors" from The Featured Areas Research Center Program within the framework of the Higher Education Sprout Project by the Ministry of Education (MOE) in Taiwan.

ORCID

Mohammad Ghalambaz https://orcid.org/0000-0003-0965-2358

REFERENCES

1. Fu J, Cano ZP, Park MG, Yu A, Fowler M, Chen Z. Electrically rechargeable zinc–air batteries: progress, challenges, and perspectives. *Adv Mater*. 2017;29(7):1604685.
2. Li Y, Dai H. Recent advances in zinc–air batteries. *Chem Soc Rev*. 2014;43(15):5257-5275.
3. Zheng F, Kotobuki M, Song S, Lai MO, Lu L. Review on solid electrolytes for all-solid-state lithium-ion batteries. *J Power Sources*. 2018;389:198-213.
4. Zou C, Zhang L, Hu X, Wang Z, Wik T, Pecht M. A review of fractional-order techniques applied to lithium-ion batteries, lead-acid batteries, and supercapacitors. *J Power Sources*. 2018;390:286-296.
5. Xue Z, Lei W, Wang Y, Qian H, Li Q. Effect of pulse duty cycle on mechanical properties and microstructure of nickel-graphene composite coating produced by pulse electrodeposition under supercritical carbon dioxide. *Surf Coat Technol*. 2017;325:417-428.
6. Wang Y, Guo R, Liu W, et al. Co_3O_4 nanospheres composed of highly interconnected nanoparticles for boosting Li-ion storage. *J Power Sources*. 2019;444:227260.
7. Li Y, Li Q, Tan Z. A review of electrospun nanofiber-based separators for rechargeable lithium-ion batteries. *J Power Sources*. 2019;443:227262.
8. Winslow KM, Laux SJ, Townsend TG. A review on the growing concern and potential management strategies of waste lithium-ion batteries. *Resour Conserv Recycl*. 2018;129:263-277.
9. Vorrath S. Is this the end of household battery storage in Australia? 2019. https://reneweconomy.com.au/is-this-the-end-of-household-battery-storage-in-australia-79766/. Accessed XX XX, XX.
10. Han X, Lu L, Zheng Y, et al. A review on the key issues of the lithium ion battery degradation among the whole life cycle. *eTransportation*. 2019;1:100005.
11. Reddy T.T. *Linden's Handbook of Batteries*. 4thNew York: . McGraw-Hill; 2010.
12. Han X, Li X, White J, et al. Metal–air batteries: from static to flow system. *Adv Energy Mater*. 2018;8(27):1801396.
13. Chang G, Cui X, Li Y, Ji Y. Effects of reciprocating liquid flow battery thermal management system on thermal characteristics and uniformity of large lithium-ion battery pack. *Int J Energy Res*. 2020;44:6383-6395. https://doi.org/10.1002/er.5363.
14. Xiaoming X, Wei T, Jiaqi F, Donghai H, Xudong S. The forced air cooling heat dissipation performance of different battery pack bottom duct. *Int J Energy Res*. 2018;42(12):3823-3836.
15. Shahid S, Agelin-Chaab M. Experimental and numerical studies on air cooling and temperature uniformity in a battery pack. *Int J Energy Res*. 2018;42(6):2246-2262.
16. Zhao R, Liu J, Gu J, Zhai L, Ma F. Experimental study of a direct evaporative cooling approach for Li-ion battery thermal

management. *Int J Energy Res*. 2020;44:6660-6673. https://doi.org/10.1002/er.5402.
17. Yang Y, Li W, Xu X, Tong G. Heat dissipation analysis of different flow path for parallel liquid cooling battery thermal management system. *Int J Energy Res*. 2020;44:5165-5176. https://doi.org/10.1002/er.5089.
18. Xie Y, Zheng J, Li W, et al. An improved electrothermal-coupled model for the temperature estimation of an air-cooled battery pack. *Int J Energy Res*. 2020;44(3):2037-2060.
19. Mutlu RN, Yazıcı B. The behavior of chemical and electrochemical Ag deposition on FeNi-mesh cathodes in Al-air battery. *Int J Energy Res*. 2019;43(12):6256-6268.
20. Trocino S, Faro ML, Zignani SC, Antonucci V, Aricò AS. High performance solid-state iron-air rechargeable ceramic battery operating at intermediate temperatures (500–650°C). *Appl Energy*. 2019;233:386-394.
21. Asadi M, Sayahpour B, Abbasi P, et al. A lithium-oxygen battery with a long cycle life in an air-like atmosphere. *Nature*. 2018;555(7697):502-506.
22. Ma J, Qin C, Li Y, Ren F, Liu Y, Wang G. Properties of reduced graphene oxide for Mg-air battery. *J Power Sources*. 2019;430:244-251.
23. Sankarasubramanian S, Kahky J, Ramani V. Tuning anion solvation energetics enhances potassium-oxygen battery performance. *Proc Natl Acad Sci*. 2019;116(30):14899-14904.
24. Wang HF, Tang C, Zhang Q. A review of precious-metal-free bifunctional oxygen electrocatalysts: rational design and applications in Zn-air batteries. *Adv Funct Mater*. 2018;28(46):1803329.
25. Wu Z, Zhang H, Guo C, et al. Effects of indium, gallium, or bismuth additions on the discharge behavior of Al-Mg-Sn-based alloy for Al-air battery anodes in NaOH electrolytes. *J Solid State Electrochem*. 2019;23(8):2483-2491.
26. Zhu C, Yang H, Wu A, Zhang D, Gao L, Lin T. Modified alkaline electrolyte with 8-hydroxyquinoline and ZnO complex additives to improve Al-air battery. *J Power Sources*. 2019;432:55-64.
27. Wang Y, Pan W, Kwok HY, Zhang H, Lu X, Leung DY. Liquid-free Al-air batteries with paper-based gel electrolyte: a green energy technology for portable electronics. *J Power Sources*. 2019;437:226896.
28. Ko J, Kwon H, Im D. Metal-air battery having air supply module and method of operating the metal-air battery. Google Patents; 2019.
29. Ko J, Kwon H, Im D. Metal-air battery having air purification module and method of operating the metal-air battery. Google Patents; 2018.
30. Ko J, Kwon H. Metal air battery having air purification module, electrochemical cell having air purification module and method of operating metal air battery. Google Patents; 2019.
31. Manthiram A, Li L. Metal-air battery. Google Patents; 2018.
32. Sagou F, Yamashita S, Nishihara M. Flow battery. Google Patents; 2020.
33. Amendola S, Johnson L, Binder M, et al. Electrically rechargeable, metal-air battery systems and methods. Google Patents; 2018.
34. Kear G, Shah AA, Walsh FC. Development of the all-vanadium redox flow battery for energy storage: a review of technological, financial and policy aspects. *Int J Energy Res*. 2012;36(11):1105-1120.
35. Yuan XZ, Song C, Platt A, et al. A review of all-vanadium redox flow battery durability: degradation mechanisms and mitigation strategies. *Int J Energy Res*. 2019;43(13):6599-6638.
36. Linden D, Reddy T. *Handbook of Batteries*. 3rd ed.New York: McGraw-Hill; 2008.
37. Koscher G, Kordesch K. Can refillable alkaline methanol-air systems replace metal-air cells? *J Power Sources*. 2004;136(2):215-219.
38. Bruce PG, Freunberger SA, Hardwick LJ, Tarascon J-M. Li-O_2 and Li-S batteries with high energy storage. *Nat Mater*. 2012;11(1):19.
39. Mainar AR, Leonet O, Bengoechea M, et al. Alkaline aqueous electrolytes for secondary zinc-air batteries: an overview. *Int J Energy Res*. 2016;40(8):1032-1049.
40. Mainar AR, Iruin E, Colmenares LC, et al. An overview of progress in electrolytes for secondary zinc-air batteries and other storage systems based on zinc. *J Energy Storage*. 2018;15:304-328.
41. Wang K, Yu J. Lifetime simulation of rechargeable zinc-air battery based on electrode aging. *J Energy Storage*. 2020;28:101191.
42. Chladil L, čech O, Smejkal J, Vanýsek P. Study of zinc deposited in the presence of organic additives for zinc-based secondary batteries. *J Energy Storage*. 2019;21:295-300.
43. Li N, Gao C-H, Yang S-Z. Preparation and structure of nanocrystalline Ni-Mo alloy coating by electrodeposition in alkaline solution. *Trans Mater Heat Treat*. 2008;6.http://en.cnki.com.cn/Article_en/CJFDTotal-JSCL200806034.htm.
44. Zhang H, Xu J-J, Chen H-Y. Shape-controlled gold nanoarchitectures: synthesis, superhydrophobicity, and electrocatalytic properties. *J Phys Chem C*. 2008;112(36):13886-13892.
45. Li L-L, Chang C-W, Wu H-H, Shiu J-W, Wu P-T, Diau EW-G. Morphological control of platinum nanostructures for highly efficient dye-sensitized solar cells. *J Mater Chem*. 2012;22(13):6267-6273.
46. Yang T-F, Lu J-H, Yan W-M, Ghalambaz M. Optimization of pulse current on energy storage of zinc-air flow batteries. *J Power Sources*. 2019;442:227253.
47. Taguchi G. *Introduction to Quality Engineering*. Tokyo: Asian Productivity Organization; 1990.
48. Freddi A, Salmon M. Introduction to the Taguchi Method. *Design Principles and Methodologies*. Springer; 2019.159–180. https://link.springer.com/chapter/10.1007/978-3-319-95342-7_7.
49. Yang WP, Tarng Y. Design optimization of cutting parameters for turning operations based on the Taguchi method. *J Mater Process Technol*. 1998;84(1–3):122-129.

How to cite this article: Yang T-F, Chen J-C, Yan W-M, Ghalambaz M. Optimization of the zinc oxide reduction in the charging process of zinc-air flow batteries. *Int J Energy Res*. 2020;44:8399–8412. https://doi.org/10.1002/er.5520